

## He II $P_\alpha$ Stark broadening and intensity ratio of C IV and C III lines calibrated with Thomson scattering for high-density plasma diagnostics

A. Gawron, S. Maurmann, F. Böttcher, A. Meckler, and H.-J. Kunze

*Institut für Experimentalphysik V, Ruhr-Universität Bochum, Postfach 102148, 4630 Bochum 1, West Germany*

(Received 29 February 1988)

With the help of Thomson scattering diagnostics we have measured the density dependence of the He II  $P_\alpha$  (468.6 nm) full half-width up to  $n_e = 2.2 \times 10^{24} \text{ m}^{-3}$  and the temperature dependence of the intensity ratio of the C IV (116.9 nm) and C III (117.6 nm) vacuum-uv lines from 9 to 13 eV. We also present a ready-to-use graphical method for the determination of electron density and temperature from the ion feature of the coherent  $90^\circ$  Thomson scattering ( $\alpha \gg 1$ ) from high-density hydrogen plasmas.

### I. INTRODUCTION

For the investigation of high-density plasmas a reliable and easy-to-use diagnostic method is desirable. One possibility for the electron density determination of plasmas containing traces of ionized helium offers the measurement of the full width at half maximum (FWHM) intensity of the He II  $P_\alpha$  line at 468.6 nm.<sup>1</sup> A favorable characteristic of this spectral line for this purpose is the weak temperature dependence. For electron densities of the order of  $n_e \approx 10^{24} \text{ m}^{-3}$ , this theoretically predicted variation of the FWHM is less than 5% in the range  $2 \leq kT_e \leq 16 \text{ eV}$ .<sup>2</sup>

Pittman and Fleurier<sup>1,3</sup> have proposed a semiempirical relationship between the FWHM of the He II  $P_\alpha$  line and the electron density  $n_e$  given by

$$n_e = 3.31(\Delta\lambda_{\text{FWHM}}/\text{nm})^{1.21} \times 10^{23} \quad (1)$$

in  $\text{m}^{-3}$ . This relation agrees very well with the results of calculations by Griem and Shen.<sup>4</sup> There seems to be no substantial deviation of measurements from Eq. (1) in the density range of  $3 \times 10^{22} \text{ m}^{-3} \leq n_e \leq 6 \times 10^{23} \text{ m}^{-3}$ ; on the other hand, the only measurements at electron densities higher than  $n_e = 6 \times 10^{23} \text{ m}^{-3}$  indeed deviate systematically,<sup>5</sup> and for this reason, we have measured the FWHM of the He II  $P_\alpha$  line for independently determined electron densities between  $1 \times 10^{24}$  and  $2.2 \times 10^{24} \text{ m}^{-3}$ .

Intensity ratios of lines are sensitive functions of temperature provided the upper levels involved are separated in energy by an amount comparable with or larger than  $kT_e$ . If, in addition, suitable transitions close in wavelength can be found even the relative sensitivity calibration of the spectroscopic equipment can be avoided. For the temperature range  $7 \text{ eV} \leq kT_e \leq 17 \text{ eV}$  such lines are the multiplets  $2s2p^3P^0 - 2p^2^3P$  at 117.57 nm in C III and  $3d^2D - 4f^2F^0$  at 116.89 nm in C IV. For densities above  $n_e \approx 10^{23} \text{ m}^{-3}$  the upper level of the C III line is in LTE (local thermodynamic equilibrium) with respect to the ground state of these ions, and the upper level of the C IV line is in LTE with respect to the C V ions.<sup>6</sup> The ground states themselves are connected via two corona equations.<sup>6</sup> At densities above  $n_e \approx 10^{23} \text{ m}^{-3}$  this coronal ap-

proximation starts to break down, complete LTE between both respective upper levels being reached at about  $n_e \approx 10^{26} \text{ m}^{-3}$ .

Up to now only theoretically calculated intensity ratios have been available. We have attempted, therefore, also to calibrate the above intensity ratio with independently determined temperatures.

One of the most accurate methods to determine the temperature as well as the electron density uses Thomson scattering of intense laser radiation by the plasma electrons.<sup>7</sup> In addition, this method yields rather spatially resolved plasma parameters. The plasma source used is the gas-liner pinch, which emits the lines of interest from a rather homogeneous plasma region,<sup>8-10</sup> thus eliminating uncertainties introduced by the boundary.

### II. EXPERIMENTAL SETUP

The schematic of the experimental setup is shown in Fig. 1. The gas-liner pinch is a modified  $z$  pinch and was extensively described previously.<sup>8-10</sup> Two fast valves inject two different kinds of gas into the discharge chamber. The so-called driver gas streams as a shell concentrically to the axis with a radius of 9 cm. The second gas (test gas) flows along the axis. The driver gas absorbs the energy from the outer circuit and is accelerated by the magnetic piston toward the center, where it forms the plasma. If the amount of test gas is well below the driver gas ( $\approx 1\%$  of the driver gas), the test gas can be considered as a mere impurity of the plasma formed by the driver gas. The test gas ions remaining in the center of the plasma column are therefore emitting radiation without self-absorption effects at a cold boundary and are emitting only from a region with rather homogeneous plasma parameters;<sup>11</sup> thus, no Abel inversion is necessary. These advantages have been used already in several line-broadening studies.<sup>11-13</sup>

The main parameters of the gas-liner pinch are 5-cm distance between the electrodes, 18-cm diameter of the discharge chamber, 3.5 kJ stored energy, 6.5- $\mu\text{s}$  period of the discharge, and a duration of the monitored continuum radiation of about 250 ns (measured between half-intensity points).

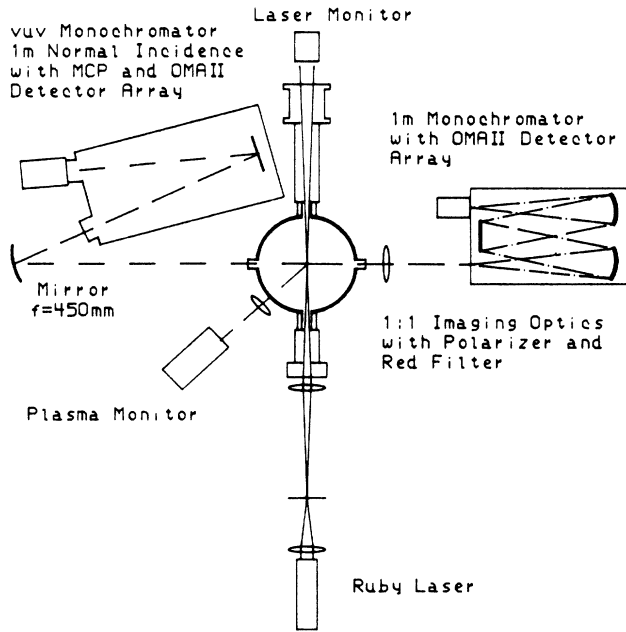


FIG. 1. Experiment setup.

The light source for the  $90^\circ$  Thomson scattering diagnostic was a Korad  $Q$ -switch-driven ruby laser (K-1Q), emitting a light pulse of 20-ns duration and 2.5 J energy at 694.3 nm. We have used a temperature-controlled resonance etalon to decrease the FWHM of the spectral distribution of the laser light to less than 0.01 nm. The laser was focused through a system of diaphragms into the center of the discharge chamber to a diameter of 1 mm. After passing a beam dump, the laser light was monitored with a FND-100 photodiode to check the reproducibility of the laser and the timing.

The visible spectral region was recorded with a 1-m monochromator (SPEX No. 1704 with a 1200-lines/mm grating blazed at 500 nm). The dispersed light at the exit slit was observed with a pulsed OMAII detector array (EG&G model 1420, pulsed for 50 ns) with 700 sensitive channels. The reciprocal dispersion of this system was 0.02 nm/channel. The apparatus profile was found to be almost Lorentzian with 0.08 nm FWHM in first order of the system.

The vacuum-uv region was observed with a 1-m normal-incidence spectrometer (McPherson model 225) with a concave grating of 1200 lines/mm. The reciprocal dispersion was 0.83 nm/mm with an entrance slit of 25  $\mu\text{m}$ . Due to the pulsed gas inlet of the gas-liner pinch no differential pumping equipment was necessary. A concave mirror was used to image the plasma column onto the entrance slit.

In the exit slit plane we mounted a microchannel plate of the chevron type (Galileo model 3025) with CsI coating on the input side and a P20 phosphor at the exit side. This phosphor screen was imaged onto the sensitive area of a second OMA II detector head. To achieve time resolution we gated the first plate of the chevron pair with a nearly rectangular voltage pulse of  $-700$  V and a duration of 30 ns; this gate pulse was simultaneous to that of

the OMA system for the visible spectral region.

The reciprocal dispersion of this detection system was 0.0209 nm/channel in first order. The apparatus profile was approximated by a Voigt profile with 0.005-nm Gaussian and 0.085-nm Lorentzian FWHM in second order. A detailed description of the vacuum-uv detection system can be found in Ref. 12.

In order to judge the reproducibility of the discharge, we monitored the radiation of the plasma column at 520 nm with a 1/4-m monochromator equipped with a RCA 1P28 photomultiplier. The signals from the laser monitor, the plasma monitor, and the gating pulses from the OMA II detection systems allowed us to achieve a time correlation between these components.

### III. THOMSON SCATTERING

For high-density, low-temperature plasmas as produced in our pinch device ( $n_e \leq 2 \times 10^{24} \text{ m}^{-3}$ ,  $kT_e \leq 15$  eV), the regime of collective Thomson scattering characterized by the plasma parameter  $\alpha > 1$  is reached with a ruby laser as light source even for a scattering angle of  $90^\circ$ . The parameter  $\alpha$  is given in this case by

$$\alpha = 1.06 \times 10^{-11} \left[ \frac{n_e (\text{m}^{-3})}{kT_e (\text{eV})} \right]^{1/2}. \quad (2)$$

Compared with the scattering intensity of the ion feature, the electron feature was too weak to be observable with the 125-MW ruby laser we used because it was masked by fluctuations of the strong plasma continuum radiation. The plasma parameters thus had to be deduced solely from the ion feature.

The complete scattering arrangement was calibrated utilizing Rayleigh scattering in a gas.<sup>7</sup> For this purpose we filled the discharge chamber with propane gas at different pressures to accomplish both the sensitivity calibration and a check of the linearity of the OMA II detection system in the visible spectral region. The observed spectral distribution of the Rayleigh-scattered light was found to be identical with the apparatus profile of the detection system.

Typical scattering signals from a pure hydrogen plasma and from propane gas observed with our arrangement are shown in Fig. 2. For the plasma parameter determination from the ion feature we developed a convenient graphical method: we use the FWHM of the ion feature and its wavelength-integrated intensity as input parameter for this method because these data can be obtained readily and with sufficient accuracy from the spectra.

The experiment yields the product  $n_e S_i(\mathbf{k})$  (see Ref. 7)

$$n_e S_i(\mathbf{k}) = n_R \left[ \frac{\sigma_R}{\sigma_{\text{Th}}} \right] \left[ \frac{W_s}{W_R} \right] \left[ \frac{L_R}{L_s} \right], \quad (3)$$

where  $\mathbf{k}$  is the scattering vector,  $S_i(\mathbf{k})$ , the ion component of form factor,  $W$ , the wavelength-integrated scattering intensity in arbitrary units,  $L$ , the time-integrated laser intensity in arbitrary units,  $n_R$ , the number of gas molecules per  $\text{m}^{-3}$ ,  $\sigma_R$ , the Rayleigh cross section, and the Thomson cross section is  $\sigma_{\text{th}} = 6.65246 \times 10^{-29} \text{ m}^2$ . The indices  $s$  and  $R$  denote Thomson

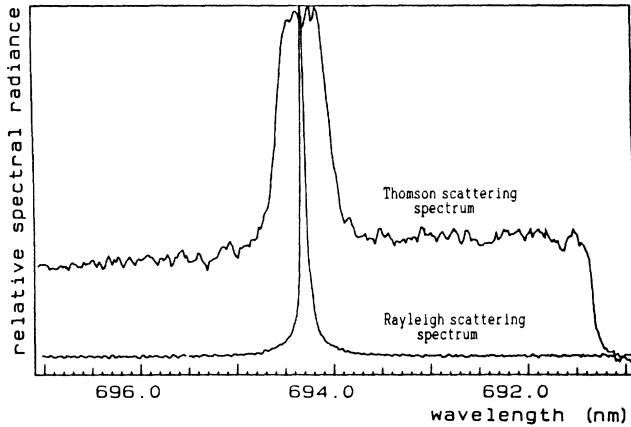


FIG. 2. Ion component of the spectrum of Thomson-scattered light and Rayleigh light scattering spectrum, both normalized to maximum intensity.

scattering and Rayleigh scattering, respectively.

At high densities, electron and ion temperatures typically are equal because of the fast electron-ion collision rate, and the component  $S_i(\mathbf{k})$  of the form factor may readily be calculated in the Salpeter approximation.<sup>14,15</sup> It is given by

$$S_i(\mathbf{k}) = \frac{1}{1 + \alpha^2} \frac{Z\alpha^4}{1 + \alpha^2 + Z\alpha^2}, \quad (4)$$

where  $Z$  is the ionic charge of the plasma ions. The FWHM is taken from theoretical spectra  $S(\mathbf{k}, \omega)$  (see Ref. 15, Eq. 7.2.1). Figure 3 shows the relation between this FWHM and the temperature for various values of the parameter  $n_e S_i(\mathbf{k})$  for a hydrogen plasma with  $Z=1$ . Figure 4 displays the corresponding relation between the temperature and the plasma parameter  $\alpha$ . The FWHM of Fig. 3 does not include any apparatus profile. In the evaluation of our data we have taken into account the ap-

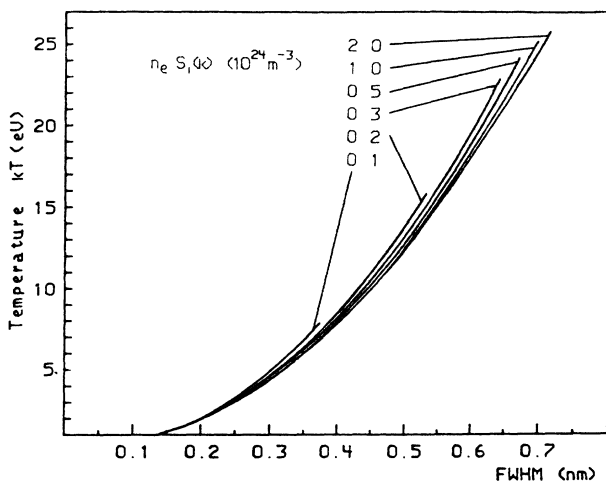


FIG. 3. Electron temperature and  $n_e S_i(\mathbf{k})$  dependence of the full half-width (FWHM) of the ion feature in the case of collective Thomson scattering from a hydrogen plasma with  $T_e = T_i = T$  and  $\Theta = 90^\circ$ .

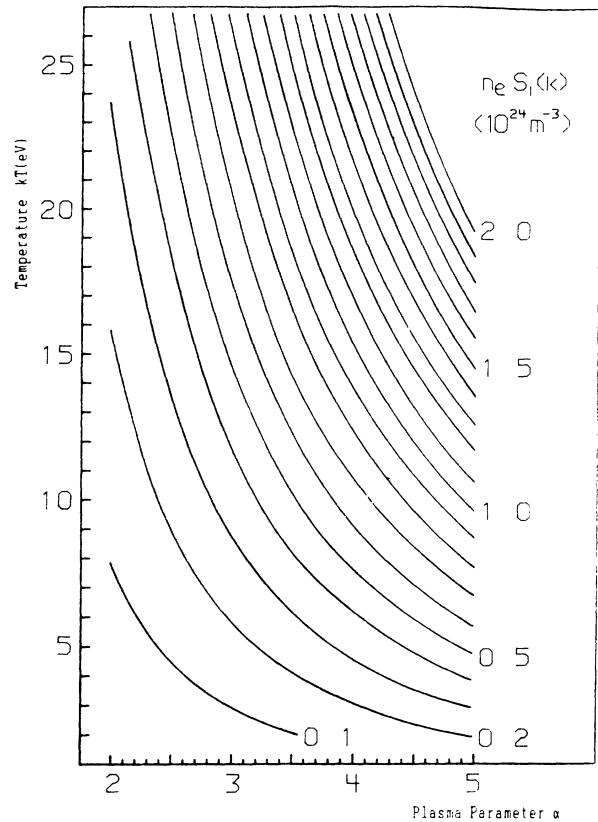


FIG. 4. Dependence of the plasma parameter  $\alpha$  on the electron temperature  $kT_e$  and the product  $n_e S_i(\mathbf{k})$  for the case of collective Thomson scattering from a hydrogen plasma,  $T_e = T_i = T$  and  $\Theta = 90^\circ$ .

paratus profile which is given by the profile of the Rayleigh-scattered light (see Fig. 2). Although the FWHM of this apparatus profile amounts to about 10% or more of the width of ion component  $S_i(\mathbf{k}, \omega)$  the convolution of both profiles does not change the FWHM of the ion component by more than 3% due to its special shape.

With the experimental FWHM of the ion component and its "intensity"  $n_e S_i(\mathbf{k})$  the temperature is now readily deduced from Fig. 3, and with this temperature the plasma parameter  $\alpha$  from Fig. 4. The electron density finally is obtained from Eq. (2), which may be written as

$$n_e / \text{m}^3 = 8.89 \times 10^{21} \alpha^2 \quad (5)$$

in kT/eV.

A detailed comparison of the shape of the ion component with theoretical spectra verifies our assumption that electron and ion temperatures indeed are equal.

The theoretical calculations of the spectra assume a fully ionized hydrogen plasma. At low temperatures, however, Rayleigh scattering from excited hydrogen atoms becomes important and may mask considerably the ion component of the spectrum. Maurmann and Kunze<sup>16</sup> have investigated this effect, and Fig. 1 of Ref. 16 gives the intensity ratio of the Rayleigh-scattered light and the ion component for a scattering arrangement as used in this investigation; this figure may be used to

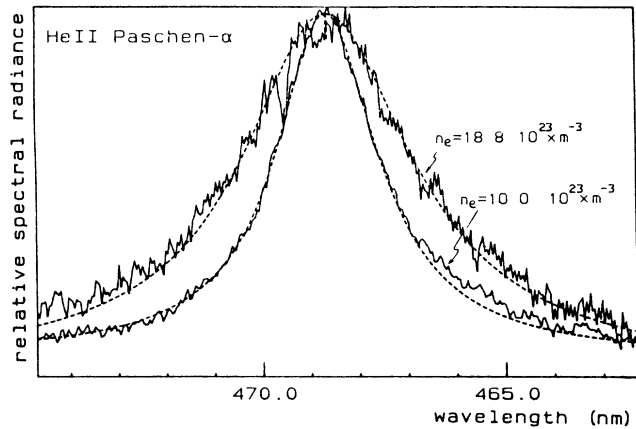


FIG. 5. He II  $P_\alpha$  line at two different electron densities at about 13 eV, normalized to maximum intensity. The dashed lines are Voigt profiles including apparatus Doppler, and a Lorentzian profile. The density values shown in the figure were calculated from the half-width (FWHM) with Eq. (1).

correct the data.

For the spectroscopic investigations test gases admitted to the gas-liner pinch were helium and methane, hydrogen being the driver gas in both cases. The amount of test gas was kept low enough as not to influence the

shape of the ion component; we compared measured scattering spectra with and without test gas, and no noticeable difference was observed within the error bars resulting from plasma continuum fluctuations. Theoretical calculations by Evans<sup>17</sup> confirm our neglect of the influence of impurities: helium and carbon impurities of the order of 1% of the hydrogen plasma do not modify sufficiently the theoretical spectra at our plasma conditions.

#### IV. RESULTS AND DISCUSSION

Two of the profiles of the He II  $P_\alpha$  line measured at different times after maximum compression of the plasma thus corresponding to different electron densities are shown in Fig. 5. The underlying continuum radiation was subtracted. This can be conveniently done by recording the continuum without the injection of the test gas. The profiles are superpositions of about 5–10 single shot spectra, which are somewhat more noisy but have the same FWHM and are measured for the same plasma parameters. To extract the FWHM from the profiles due to Stark broadening, we have fitted Voigt profiles including apparatus broadening and Doppler broadening to the measured profiles.

The FWHM's determined in this way are plotted

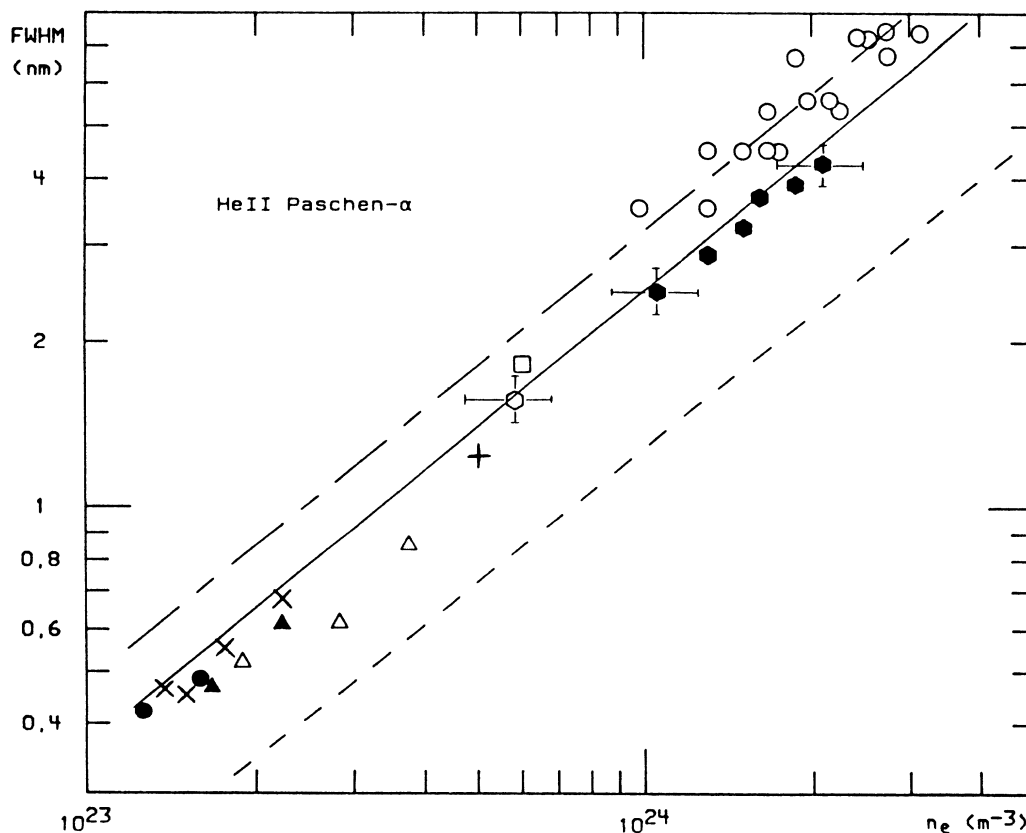


FIG. 6. Comparison of measurements of the full half-width of the He II  $P_\alpha$  line at 468.6 nm with theory as a function of electron density. Theoretical calculations are from Greene (Ref. 23) — — —; Kepple (Ref. 24), - - - -; and from Griem and Shen (Ref. 4) — — —. The experimental data are as follows:  $\times$ , Ref. 1;  $\circ$ , Ref. 11;  $\square$ , Ref. 18;  $\triangle$ , Ref. 19;  $\blacktriangle$ , Ref. 20;  $\circ$ , Ref. 5;  $+$ , Ref. 21;  $\bullet$ , Ref. 22;  $\bullet$ , present measurements.

versus the electron density obtained from Thomson scattering in Fig. 6. This figure is taken from Ref. 1; experimental data from Ref. 11 and our measurements are included in addition, revealing very good agreement with Eq. (1) and the calculations by Griem and Shen.<sup>4</sup> These early calculations neglect both ion dynamics and the so-called upper-lower state interference term,<sup>25,26</sup> whose effects tend to counteract each other in the determination of the spectral linewidth. It is clear<sup>13</sup> that inclusion of only one or the other of these would lead to appreciable errors in the calculated hydrogenic linewidths, as, for example, in the results of Greene<sup>23</sup> shown in Fig. 6. It is possible that with inclusion of both effects under discussion improvements to the calculations of Kepple<sup>24</sup> would lead to even better agreement with our experimental results.

Because we could not perform Thomson scattering diagnostics and the measurement of the  $P_\alpha$  line at the same time, the error bars in Fig. 6 take into account the reproducibility of the pinch discharge as well as the accuracy of our diagnostics. The variation of the electron density between  $n_e = 1 \times 10^{24}$  and  $2.2 \times 10^{24} \text{ m}^{-3}$  was obtained by simply making the spectroscopic observations at different times of the pinch discharge; the electron temperature dropped from 13 eV at the higher density to 9 eV at the lower one. The uncertainty of the measurement is less than 20% (15% due to the Thomson scattering, 10% reproducibility of the pinch discharge) for the electron density and about 10% for the full half-width of the He II  $P_\alpha$  line profile, neglecting the temperature dependence of the  $P_\alpha$  width.<sup>2</sup> It was shown previously<sup>3</sup> that the Balmer- $\alpha$  line of He II was optically thin for the same plasma conditions; hence it can safely be assumed that the Paschen- $\alpha$  line is optically thin, too.

Measurements of the He II  $P_\alpha$  FWHM in a density range of  $1 \times 10^{24} \leq n_e \leq 3 \times 10^{24} \text{ m}^{-3}$  were also reported by Jones *et al.*<sup>5</sup> Their measurements are represented in Fig. 6 by open circles. They used a  $\theta$ -pinch discharge with a pure helium filling and determined the electron density from the absolute value of the continuum intensity and a total sweep up compressional model calculation. The line profile was scanned on a shot-to-shot basis. A recently done comparison between their results and theory can be found in Ref. 27. Their profiles are consistently wider than predicted by Eq. (1) by about 30%.

Figure 7, finally, shows the experimental intensity ratios of the C IV line at 116.9 nm and the C III line at 117.6 nm versus the temperature obtained from Thomson scattering. The solid line represents the theoretical temperature dependence of the intensity ratio, which is essentially the calculation from Ref. 6 adopted to the present transitions; the transition probabilities used are based on the Coulomb approximation<sup>28</sup> for the C IV lines and are taken from Ref. 29 for the C III lines. (See Ref. 13 for a more detailed description of the calculation.) The calculations presume optically thin lines. In our case, this was checked by comparing the measured line intensity with the blackbody-limited intensity of an optically thin C IV line ( $2s-2p$ ).<sup>12</sup>

The experimental points shown in Fig. 7 are mean values of about 10–20 single shots, the uncertainties of

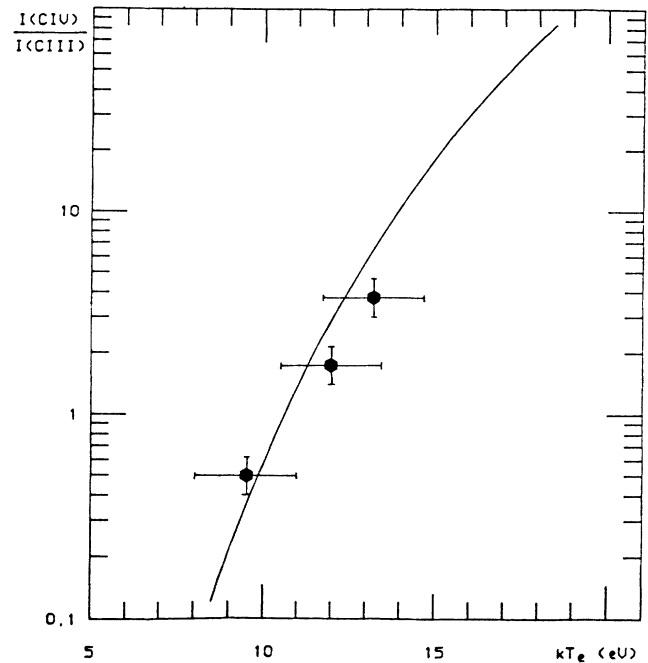


FIG. 7. Theoretical temperature-dependent ratio of the wavelength-integrated intensity  $I(\text{CIV } 116.9 \text{ nm})/I(\text{CIII } 117.6 \text{ nm})$  compared with our measurements.

about 1.5 eV in the temperature and 20% in the intensity ratio are including the statistical deviation of the single shot and any uncertainty in the determination of the temperature and intensity ratio for a single shot. Examples of measured vacuum-uv spectra can be seen in Fig. 2 of Ref. 13. We have to point out that the measurements were made at densities of about  $2 \times 10^{24} \text{ m}^{-3}$  which is somewhat higher than the estimated density of  $1 \times 10^{23} \text{ m}^{-3}$  where the corona approximation starts to break down (see Sec. I). The agreement between the measured values and the calculation is within the experimental uncertainties.

## V. CONCLUSION

At high densities, we have measured the FWHM of the He II  $P_\alpha$  line due to Stark broadening and determined the electron density independently and found good agreement between our results and a semiempirical relation proposed by Pittman and Fleurier<sup>1</sup> [Eq. (1)]. We conclude therefore that this relation is a good description of the Stark broadening of the He II  $P_\alpha$  line in the electron density range between  $n_e = 5 \times 10^{22} \text{ m}^{-3}$  (Fig. 4 of Ref. 1) and  $2 \times 10^{24} \text{ m}^{-3}$ .

We have also compared the intensity ratio of the C IV line at 116.9 nm and the C III line at 117.6 nm with the independently determined electron temperature. We

have found good agreement between our measurements and a theoretical derivation based on a calculation by Griem.<sup>6</sup> We conclude that this intensity ratio offers a good spectroscopic possibility to measure electron temperatures between 7 and 17 eV for plasmas with electron densities of at least up to  $2 \times 10^{24} \text{ m}^{-3}$ .

#### ACKNOWLEDGMENTS

This work was supported by the Sonderforschungsbe-  
reich 162 (Plasmaphysik Bochum/Jülich). We are ob-  
liged to Dr. K. H. Finken, Dr. J. Musielok, and Dr. J. D.  
Hey for helpful discussions.

- 
- <sup>1</sup>T. L. Pittman and C. Fleurier, *Phys. Rev. A* **33**, 1291 (1986).  
<sup>2</sup>H. R. Griem, *Spectral Line Broadening by Plasmas* (Academic, New York, 1974).  
<sup>3</sup>T. L. Pittman and C. Fleurier, in *Spectral Line Shapes*, edited by K. Burnett (deGruyter, New York, 1983), Vol. II.  
<sup>4</sup>H. R. Griem and K. Y. Shen, *Phys. Rev.* **122**, 1490 (1961).  
<sup>5</sup>L. A. Jones, E. Källne, and D. B. Thomson, *J. Quant. Spectrosc. Radiat. Transfer* **17**, 175 (1977).  
<sup>6</sup>H. R. Griem, *Plasma Spectroscopy* (McGraw-Hill, New York, 1964).  
<sup>7</sup>H.-J. Kunze, in *Plasma Diagnostics*, edited by W. Lochte-Holtgreven (North-Holland, Amsterdam, 1968).  
<sup>8</sup>K. H. Finken and U. Ackermann, *Phys. Lett.* **85A**, 279 (1981).  
<sup>9</sup>K. H. Finken and U. Ackermann, *J. Phys. D* **15**, 615 (1982).  
<sup>10</sup>K. H. Finken and U. Ackermann, *J. Phys. D* **16**, 773 (1983).  
<sup>11</sup>U. Ackermann, K. H. Finken and J. Musielok, *Phys. Rev. A* **31**, 2597 (1985).  
<sup>12</sup>F. Böttcher, J. Musielok, and H.-J. Kunze, *Phys. Rev. A* **36**, 2265 (1987).  
<sup>13</sup>J. Musielok, F. Böttcher, H. R. Griem, and H.-J. Kunze, *Phys. Rev. A* **36**, 5683 (1987).  
<sup>14</sup>E. E. Salpeter, *Phys. Rev.* **120**, 1528 (1960).  
<sup>15</sup>J. Sheffield, *Plasma Scattering of Electromagnetic Radiation* (Academic, New York, 1975).  
<sup>16</sup>S. Maurmann and H.-J. Kunze, *Phys. Fluids* **26**, 1630 (1983).  
<sup>17</sup>D. E. Evans, *Plasma Phys.* **12**, 573 (1970).  
<sup>18</sup>J. R. Bernard, D. L. Curzon, and A. S. Barnard, in *Spectral Line Shapes*, edited by B. Wende (deGruyter, Berlin, 1981).  
<sup>19</sup>T. Oda and S. Kiriya, *J. Phys. Soc. Jpn.* **49**, 385 (1980).  
<sup>20</sup>M. E. Bacon, A. J. Barnard, and F. L. Curzon, *J. Quant. Spectrosc. Radiat. Transfer* **18**, 399 (1977).  
<sup>21</sup>P. Z. Bogen, *Naturforsch.* **25a**, 1151 (1979).  
<sup>22</sup>H. F. Berg, A. W. Ali, R. Lincke, and H. R. Griem, *Phys. Rev.* **125**, 199 (1962).  
<sup>23</sup>R. L. Greene, *Phys. Rev. A* **14**, 1447 (1976).  
<sup>24</sup>P. C. Kepple, *Phys. Rev.* **6**, 1 (1972).  
<sup>25</sup>H. R. Griem and J. D. Hey, *Phys. Rev. A* **14**, 1906 (1976).  
<sup>26</sup>D. Voslamber, *Phys. Rev. A* **14**, 1903 (1976).  
<sup>27</sup>E. Källne and L. A. Jones, *J. Phys. B* **13**, L437 (1980).  
<sup>28</sup>D. R. Bates and A. Damgaard, *Philos. Trans. R. Soc. London, Ser. A* **242**, 101 (1949).  
<sup>29</sup>K. T. Cheng, Y.-K. Kim, and J. P. Desclaux, *At. Data Nucl. Data Tables* **24**, 111 (1979).